Available online at www.sciencedirect.com
SCIENCE DIRECT®
International Journal of Heat and Fluid Flow 25 (2004) 759–766
International Journal of HEAT AND FLUID FLOW
www.elsevier.com/locate/ijhff

# Development of turbulent impinging jet on a rotating disk

Y. Minagawa, S. Obi *

*Department of Mechanical Engineering, Keio University, Hiyoshi 3-14-1, Kohoku-ku, Yokohama 223-8522, Japan*

Received 9 January 2004; accepted 12 May 2004
Available online 7 July 2004

**Abstract**

We conduct detailed velocity measurements in the turbulent boundary layer, which is developed on a rotating disk opposed to a turbulent jet perpendicularly impinged onto it. The effect of rotation is remarkable in both the skew in the mean flow and in the centrifugal force. We propose a non-dimensional parameter that correlates these two effects and classifies the velocity field. We find the modification of the turbulence structure due to the disk rotation in the increase of the normal stress component in the circumferential direction. The increases in the other stress components are found to be indirect, i.e., re-distribution from the circumferential normal stress is the source of modification in the turbulence structure.


*Keywords:* Impinging jet; Turbulence boundary layer; Centrifugal force; LDA

## 1. Introduction

The impinging jet is of great importance in many engineering-relevant problems, such as the cooling, heating, and drying processes. Accordingly, a computational prediction of heat and fluid flow associated with flow impingement has long been a challenging task in turbulence modeling (Craft et al., 1993; Behnia et al., 1999). The difficulty is that the turbulence structures are not solely determined by the mean shear, but also by the stagnation and streamline curvatures that play important roles as they impose extra rates of strain. In the present study, we consider a more complicated case in which the flow is being impinged onto a rotating disk. The moving wall causes a skew of the boundary layer, and the disk rotation asserts a centrifugal force to the fluid particle attached to the wall.

From extensive experimental and numerical studies, we can fully understand some of the characteristics of the impinging jet. For example, we can achieve the maximum amount of heat transfer at the stagnation point when the distance between the jet exit and the wall is approximately five times that of the jet diameter (Gardon and Akfirat, 1965). The interaction between the free shear layer of the impinging jet and the radial wall jet, which develops after impingement, makes the problem more complicated (Cooper et al., 1993).

Many studies have focused on the boundary layer that develops on a rotating disk in the context of turbo machinery. Among these, the experiments by Little and Eaton (1994) and Itoh and Hasegawa (1994) have revealed a unique structure of the turbulent boundary layer developed on the disk. The impinging jet on a rotating disk has been used as a cooling target in gas turbines (Popiel and Boguslawski, 1974). Experiments by Brodersen et al. (1996a,b) are extensive, and provide us with practical information about the cooling problem. Itoh and Okada (1998) conducted detailed measurements on turbulent wall jet developed on a rotating disk and showed that the turbulence structure in boundary layer deviates from equilibrium state as the disk rotation speed increases.

The primary objective of our study is to deepen the knowledge of the turbulent boundary layer developed on a rotating disk through detailed measurement of mean velocity and turbulence statistics. It is also expected that the results may serve as a basis for the assessment and improvement of existing turbulence models. To this end, experiments are conducted for systematically varied conditions, i.e., the disk rotation

* Corresponding author. Tel.: +81-45-566-1499; fax: +81-45-566-1495.
*E-mail address:* obsn@mech.keio.ac.jp (S. Obi).

0142-727X/$ - see front matter © 2004 Elsevier Inc. All rights reserved.
doi:10.1016/j.ijheatfluidflow.2004.05.013

speed, measuring location and the velocity of the impinging jet, and we attempt to address the combined effect of the skew in boundary layer and centrifugal force as a function of a local parameter.

## 2. Governing equations

### 2.1. Mean flow motion

The equation of the fluid motion considered in the present study may be derived from the Reynolds-averaged Navier–Stokes equation for incompressible flow. Under the assumption of the steady flow and symmetry about the axis of rotation, the independent variables are the radial and the axial coordinates, $r$ and $z$, respectively. Taking into account the fact that the velocity components in $r$- and $z$-directions are subject to the oncoming jet velocity, $U_j$, while the tangential velocity component is introduced due to the disk rotation, we may express the non-dimensional velocity components as follows:

$$V_r = V_r^* U_j, \quad v_r = v_r^* U_j,$$
$$V_\theta = V_\theta^* R\omega, \quad v_\theta = v_\theta^* U_j,$$
$$V_z = V_z^* U_j, \quad v_z = v_z^* U_j,$$

where $R$ is the disk radius and $\omega$ the angular velocity of the disk. Upper and lower cases correspond to the mean and fluctuating velocity components, respectively. Note that the fluctuating component in tangential direction, $v_\theta$, exists regardless of the disk rotation, hence normalized by $U_j$ rather than $R\omega$. Consequently, the non-dimensional equation of radial momentum is derived:

$$V_r^* \frac{\partial V_r^*}{\partial r^*} + V_z^* \frac{\partial V_r^*}{\partial z^*} - \left(\frac{R\omega}{U_j}\right)^2 \frac{V_\theta^{*2}}{r^*} = -\frac{\partial P^*}{\partial r^*} + \frac{\nu}{U_j R}\left(\frac{\partial^2 V_r^*}{\partial r^{*2}} + \frac{1}{r^*}\frac{\partial V_r^*}{\partial r^*} + \frac{\partial^2 V_r^*}{\partial z^{*2}} - \frac{V_r^*}{r^{*2}}\right) - \left(\frac{\partial \overline{v_r^{*2}}}{\partial r^*} + \frac{\partial \overline{v_r^* v_z^*}}{\partial z^*} - \frac{\overline{v_\theta^{*2}}}{r^*}\right). \quad (1)$$

$P^*$ stands for the normalized pressure defined as $P^* = P/\rho U_j^2$, and $\nu$ denotes the kinematic viscosity of the fluid. The above equation indicates that the influence of the disk rotation directly appears in the third term on the left hand side, and its magnitude depends on the ratio of the two characteristic velocity scales, $U_j$ and $R\omega$. It should be noted that the momentum equations in $z$- and $\theta$-directions do not contain such terms that explicitly express the effect of centrifugal force.

### 2.2. Production of Reynolds stresses

The disk rotation imposes the extra rate of strain which modifies the turbulence structure of the wall jet developed on the disk. Since the rate of strain directly influences the production of turbulence, it is worth our while to review the production term of the individual Reynolds stress components:

$$P_{rr} = -2\left(\overline{v_r^2}\frac{\partial V_r}{\partial r} + \overline{v_r v_z}\frac{\partial V_r}{\partial z} - \overline{v_r v_\theta}\frac{V_\theta}{r}\right), \quad (2)$$

$$P_{\theta\theta} = -2\left(\overline{v_r v_\theta}\frac{\partial V_\theta}{\partial r} + \underline{\overline{v_\theta v_z}\frac{\partial V_\theta}{\partial z}} + \overline{v_\theta^2}\frac{V_r}{r}\right), \quad (3)$$

$$P_{zz} = -2\left(\overline{v_r v_z}\frac{\partial V_z}{\partial r} + \overline{v_z^2}\frac{\partial V_z}{\partial z}\right), \quad (4)$$

$$P_{r\theta} = -\overline{v_r^2}\frac{\partial V_\theta}{\partial r} - \underline{\overline{v_r v_z}\frac{\partial V_\theta}{\partial z}} - \overline{v_\theta v_z}\frac{\partial V_r}{\partial z} + \overline{v_r v_\theta}\frac{\partial V_z}{\partial z} + \overline{v_\theta^2}\frac{V_\theta}{r}, \quad (5)$$

$$P_{\theta z} = -\overline{v_r v_\theta}\frac{\partial V_z}{\partial r} - \overline{v_r v_z}\frac{\partial V_\theta}{\partial r} - \underline{\overline{v_z^2}\frac{\partial V_\theta}{\partial z}} + \overline{v_\theta v_z}\frac{\partial V_r}{\partial r}, \quad (6)$$

$$P_{rz} = -\overline{v_r^2}\frac{\partial V_z}{\partial r} - \overline{v_z^2}\frac{\partial V_r}{\partial z} + \overline{v_r v_z}\frac{V_r}{r} + \overline{v_\theta v_z}\frac{V_\theta}{r}. \quad (7)$$

The equations are shown in dimensional form. The terms marked by the underline contain the extra rate of strain, $\partial V_\theta/\partial z$, that appears due to the disk rotation. The terms proportional to $V_\theta/r$, such as the last term in the bracket of Eq. (2), are considered to have only secondary effect. It is clear that the $\overline{v_\theta^2}$ will be most influenced by the disk rotation among the three normal stress components, because the production term $P_{\theta\theta}$ only possesses the above-mentioned extra rate of strain. It is also expected that the shear stress components, $\overline{v_r v_\theta}$ and $\overline{v_\theta v_z}$, are modified due to the disk rotation. The influence on the production of the other components are subject to indirect effect.

## 3. Experiment

### 3.1. Rotating disk and jet

We took measurements in the turbulent boundary layer that developed on a disk with a 150 mm radius rotating about its axis, as shown in Fig. 1. A pipe for the jet flow was set perpendicular to the disk surface, with its centerline aligned to that of the disk. The inner diameter of the pipe, $D$, was 25 mm, and the distance between the pipe exit and the disk surface was $5D$, which was kept constant throughout the experiment. This configuration was selected because it is known to realize the maximum heat transfer rate at the impingement region (Gardon and Akfirat, 1965), and hence considered by a number of computational studies (e.g., Craft et al., 1993). To avoid ambient disturbance, we put the entire test rig in a box made of 1 mm-thick vinyl, with approximate dimensions of 1200 mm × 1300 mm × 2300 mm. To insure axial symmetricity, we closely monitored

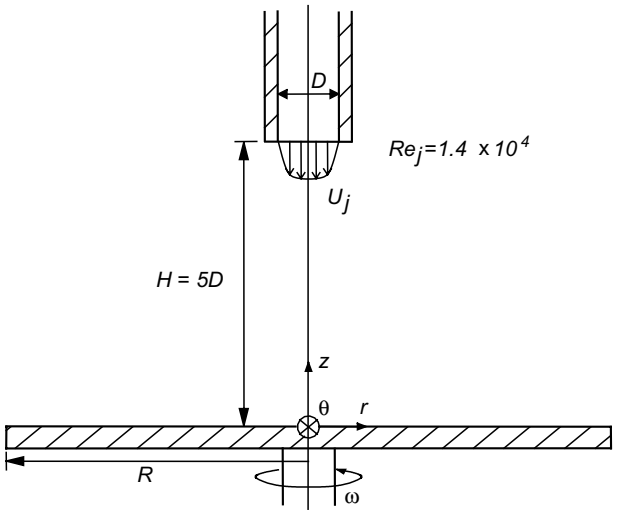


Fig. 1. Schematics of the configuration of the jet and disk.

the alignment of the pipe and the disk. The disk was mounted on a turntable unit, which was then leveled and bolted onto the laboratory floor. The pipe above the disk was adjusted using still pendulums. The estimated misalignment with respect to the vertical center line was ±0.3°.

We assumed the flow field to be axisymmetric and steady. The operating fluid was the air at room temperature, and was assumed to be incompressible. We defined a cylindrical coordinate, with an $r$ axis taken in the radial direction and a $z$ axis set normal to the disk surface.

### 3.2. Velocity measurement

We measured the velocity vectors using a one-component laser Doppler anemometer (LDA). The laser light source was an air-cooled Ar-ion Laser with a 300 mW output (Ion Laser Technology). We used a commercial transmitting optics unit (ONO SOKKI Co. Ltd., LV-5000), which operated in a backward scattering mode, that enabled flexible access to the measuring location via optical fibers, though a beam reflector was used to intensify the scattered light. The estimated dimensions of the measuring volume were 103 μm and 1.46 mm in diameter and length, respectively. We used a burst correlator (ONO SOKKI Co. Ltd., LV-5900) for data processing. Nebulae of salad oil were used as tracers, whose estimates of diameter were only a few microns.

We calculated the mean and fluctuating velocity components from 6000 data samples, which were collected from every location in the flow field. The data sampling rate varied between 50 and 150 Hz, depending on the condition. We set the integral time to 120 s at all positions, according to preliminary measurements under a typical condition ($r/D = 1.5$ and 5.0 for $x/D = 0.04$, with $\omega = 0$ and 157.1 rad/s). The difference among five measurements for every three different integral times, 120, 180, and 240 s, was found to be well below 1% in terms of the mean velocity. Hence, the integral time of 120 s was considered to be satisfactory in establishing turbulence statistics. The inevitable velocity bias in the LDA measurement was corrected using the time weighting method (Fuchs et al., 1994).

We obtained individual components of the velocity vectors, $V_r$, $V_z$, and $V_\theta$, as well as the Reynolds stress components, $\overline{v_r^2}$, $\overline{v_\theta^2}$, and $\overline{v_r v_\theta}$, etc., from a set of measurements found by the single-component LDA at every measuring location. There, the axis of the control volume was inclined at a certain angle against either the $r$- or $z$-axis so that the velocity component in the corresponding direction could be obtained. We calculated the desired velocity components and Reynolds stress components using tensor algebra.

### 3.3. Experimental condition

In order to have a fully developed turbulent pipe flow at the pipe exit, we selected a pipe length larger than $50D$, and the fully developed pipe flow profile was confirmed by the LDA measurement across the cross section at the exit. We kept the bulk velocity through the pipe, $U_j$, constant throughout the experiment at 8.70 m/s. That was so that the Reynolds number $Re_j$ based on $U_j$ and $D$ was $1.45\times10^4$, except for the examination of similarity, which will be described later. The influence of the disk rotation speed was examined for the various rotation speed $\omega$ for $0 \leqslant \omega \leqslant 167.6$ rad/s (up to 1600 rpm). This resulted in the rotational Reynolds number range for $0 \leqslant Re \leqslant 2.50 \times 10^5$, where $Re$ is defined as $R^2\omega/v$, with $R$ being the disk radius.

### 3.4. Measurement ambiguity

The most serious concern is related to the spatial coincidence of the measuring volume of three velocity measurements at the same point, which are necessary to determine the mean velocity vector and the Reynolds stress. We estimate that the ambiguity in the position of the radial direction's control volume is 220 μm, and the direction normal to the disk surface is 50 μm. This is due to the fact that the traversing apparatus needs to be adjusted whenever the direction of the measuring volume is changed. In any case, an error in the alignment of the traversing apparatus was no larger than 1°. The error in the angle was a consequence of the errors in both the location and velocity components, and changed with different measuring locations. The possible error band is given in individual graphs and will be taken into account in subsequent discussions.

## 4. Results and discussion

### 4.1. Influence of the disk rotation on the radial wall jet

The influence of disk rotation appears two-fold: The centrifugal force and the skewing of the boundary layer. The former appears explicitly in the governing equation of fluid motion, while the latter affects via boundary condition, and its effect on the turbulence structure does not appear explicitly in the equation. Hence, it is natural to conduct a parametric study focusing on the effect of the centrifugal force. In this section, we consider the influence of disk rotation by observing the radial component of the velocity, since it most directly reflects the centrifugal force.

The radial component of the mean velocity $V_r$ is given as a function of $r$ by traversing the measuring volume in the radial direction while keeping the distance from the wall constant at $z/D = 0.032$. The result is illustrated in Fig. 2, where the data obtained at three different angular velocities of the disk, $\omega = 52.4$ rad/s, 104.7 rad/s, and 157.1 rad/s, are compared with those measured for the condition of the stationary disk. The horizontal and vertical axes are normalized by the inlet conditions, $D$ and $U_j$, respectively. It is clear that the $V_r$ vanishes at the disk center, where $r = 0$, and rapidly increases to its maximum around $r/D = 1.0$, before gradually reducing due to the entrainment of the surrounding fluid and spreading in the circumferential direction. The turbulent intensity $v'_r/U_j$, with $v'_r \equiv \sqrt{\overline{v_r^2}}$, shown in Fig. 2(b), is also minimum at the disk center, and increases outwardly from the center. It reaches its maximum at $r/D \sim 2.2$ before diminishing further downstream. There is a characteristic plateau in the region $1 \leqslant r/D \leqslant 2$, and this flow pattern is consistent with the results obtained by Cooper et al. (1993).

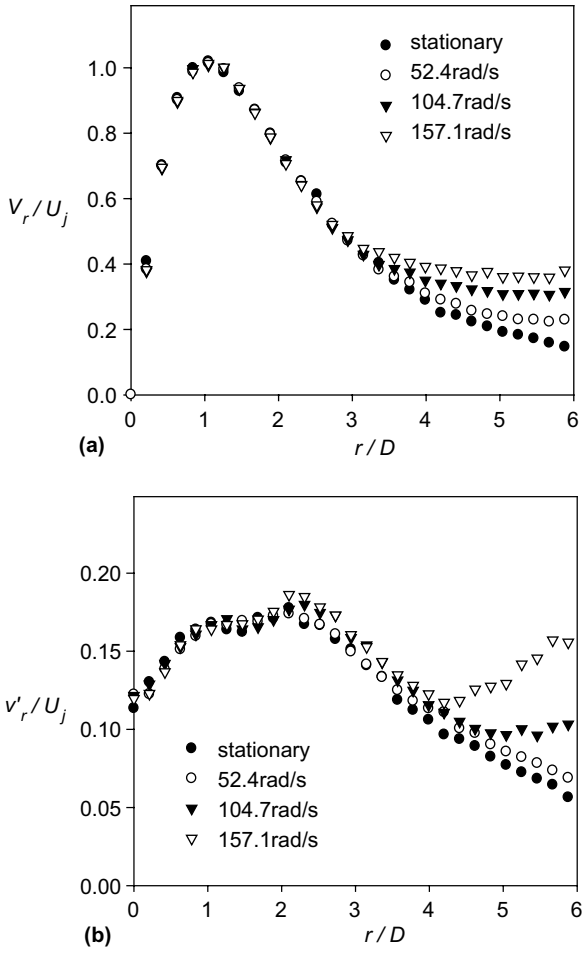


Fig. 2. Radial distribution of the near-wall radial velocity ($z/D = 0.032$): (a) mean velocity component, (b) turbulent intensity.

Comparing the plots for the stationary disk described above with those for the rotating disk, one can see that the influence of the disk rotation appears in a region away from the disk center, where the decrease in the mean velocity $V_r$ becomes less significant. This tendency becomes more obvious at a higher rotational speed, and the deviation from the plots of the stationary disk measurements starts around $r/D \sim 3.0$ for the highest rotational speed in our experiment. We observed a similar tendency in the distribution of the turbulent intensity, where we found that the influence of the disk rotation is more significant in the increase of $v'_r/U_j$ in the region $4 \leqslant r/D$ for $\omega = 157.1$ rad/s.

The above observation is readily understood as the consequence of the centrifugal force that increases with the rising circumferential velocity component, which is realized by increasing either the rotational speed or the radius. In order to clarify the relative effect of the centrifugal force, we now consider its order of magnitude. The equation of motion in the radial direction, Eq. (1), suggests that the order of the centrifugal force is determined by the ratio of the circumferential- and radial-velocity components, i.e., $V_\theta/V_r$, where the $V_\theta$ on the wall is equal to $r\omega$. Considering that the decrease of radial velocity component $V_r$ is $\propto 1/r$, a local velocity ratio $\alpha$ can be written as:

$$\alpha = \frac{r\omega}{U_j/(r/D)} = \frac{r^2\omega}{U_j D}. \tag{8}$$

In our study, the parameter $\alpha$ is expected to be a parameter that specifies the effect of the centrifugal force.

In order to investigate the validity of the parameter $\alpha$ as a scaling parameter, we have conducted a series of measurements. Since the radial velocity $V_r$ varies with $z$ in the boundary layer, and the thickness of the boundary layer varies in the $r$-direction, a simple re-scaling of the data presented in Fig. 2 does not make sense. To obtain a better similarity of the velocity profile, we take the re-scaling in terms of the variation of $V_{r\max}$, the maximum value of $V_r$, where $V_r$ is a function of the $z$-coordinate, and its values are then obtained for various conditions,

Table 1
Conditions for maximum $V_r$ measurements

| $r/D$ | $\omega$ (rad/s) | $U_j$ (m/s) |
|---|---|---|
| 4.5 | 62.8, 157.1 | 5.8 |
| 5.0 | 41.9, 83.8, 167.6 | 5.8 |
| 5.8 | 20.9, 41.9, 83.8, 125.7, 167.6 | 5.8 |
| 5.0 | 41.9, 83.8, 125.7, 167.6 | 6.53 |

as summarized in Table 1. The scales are in reference to $\alpha$. The results are presented in Fig. 3. It is seen that all plots fall on a single curve for both mean velocity (a), and turbulent intensity (b), where $v'_r$ measured at the same position as $V_{r\max}$; they are normalized by the values measured without disk rotation at the same radial location, $V_{r0}$ and $v'_{r0}$, respectively.

From the above observation, $\alpha$, given by Eq. (8), is proven to be a parameter that describes the effects of the centrifugal force on the wall jet developed on the rotating disk. However, the function relationship is somehow different for the mean velocity and the turbulent intensity. In Fig. 3(a), the influence of the centrifugal force becomes obvious for $4.7 \leqslant \alpha$, where $V_{r\max}$

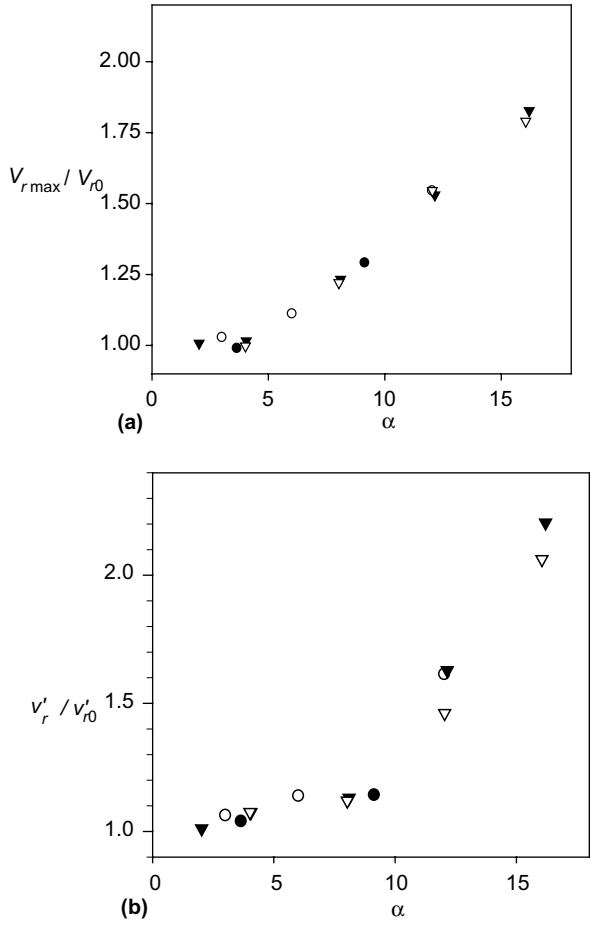


Fig. 3. Radial velocity as a function of parameter $\alpha$: (a) maximum $V_r$ at each condition, (b) turbulent intensity at the location of maximum $V_r$.

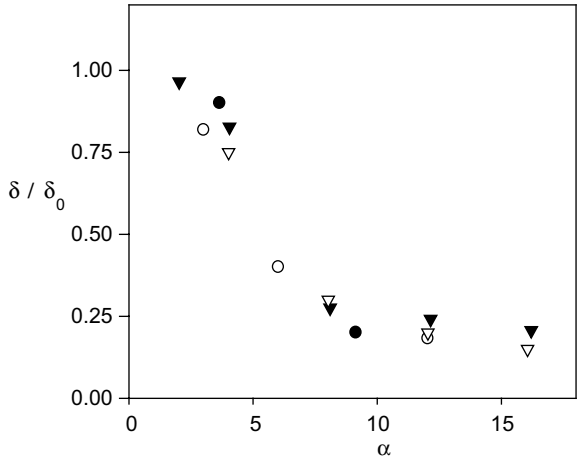


Fig. 4. Location of the maximum $V_r$ as a function of parameter $\alpha$.

starts to increase nearly proportionally to $\alpha$, while the turbulent intensity begins to increase from $\alpha \sim 2.5$, as illustrated in Fig. 3(b). A remarkable transition is also found at $\alpha \sim 9.2$, where $v'_r$ starts to increase at a higher rate. In addition, Fig. 4 shows that the $z$-coordinate for the location of $V_{r\max}$, $\delta$, is examined against $\alpha$. $\delta$ is normalized by $\delta_0$ that is obtained from the measurement without disk rotation. It is evident that the location of the maximum in wall jet is already shifted toward the wall at $\alpha = 2.0$, which is the lowest value that can be achieved by our current facility. The location of the maximum velocity ceases to move for $10 \leqslant \alpha$, which is likely to be attributable to the spatial resolution of the LDA. Nevertheless, the flow condition varies according to the parameter $\alpha$, and it seems that there are three regimes of flow pattern in terms of $\alpha$: The region with a weak effect of the centrifugal force, $\alpha \leqslant 4.7$, the intermediate region, $4.7 \leqslant \alpha \leqslant 9.2$, and the extreme condition, $9.2 \leqslant \alpha$. We discuss the detailed velocity distribution and the turbulence structure in the subsequent section.

It should be noted, however, that the similarity with respect to the parameter $\alpha$ holds only under certain conditions. For example, the impinging region where $V_r$ increases with $r$, cf. Fig. 2(a), cannot be described by Eq. (8) that assumes the decrease of $V_r$ with $r$. On the other hand, the impingement distance $H$ may also influence the above-mentioned functional relationship. For the larger $H$, the deceleration of jet velocity would occur before the impingement on the disk, so that the effect of the centrifugal force would become more obvious at smaller $\alpha$ than in the present case. The limit of $H \to \infty$ realizes a rotating disk in still ambient where the centrifugal force is the only driving force; the flow characterization in terms of $\alpha$ would have no sense in that case. On the other hand, for smaller $H$, the effect of impingement would become more obvious, resulting in a strong flow acceleration in radial direction. As a consequence, the decay of $V_r$ would be postponed and the

Table 2
Parameters for velocity measurements

| $\alpha$ | $\omega$ (rad/s) | $r/D$ ($r$ (mm)) | $Re_r$ | $U_j$ (m/s) |
|---|---|---|---|---|
| 4.0 | 41.8 | 5.8 (145) | $5.8\times10^4$ | 8.7 |
| 8.1 | 83.8 | 5.8 (145) | $1.2\times10^5$ | 8.7 |
| 16.2 | 167.6 | 5.8 (145) | $2.3\times10^5$ | 8.7 |

relative influence of $V_\theta$ might become weaker for the same value of $\alpha$ as in the present case. In any way, it is natural to expect a certain transition of flow structure as long as both the decay of $V_r$ and increase of $V_\theta$ occur with the increasing $r$, yet the generality of parameter $\alpha$ is an open question.

### 4.2. Mean velocity and Reynolds stress in the wall jet

Based on the above discussion, we measured the detailed velocity profiles under three different conditions in terms of parameter $\alpha$. The conditions are summarized in Table 2.

#### 4.2.1. Mean velocity components

The radial component $V_r$ and the circumferential component $V_\theta$ of the mean velocity are given in Fig. 5. They are respectively normalized by the jet exit velocity $U_j$ and the local circumferential velocity $r\omega$. The distance from the disk, $z$, is normalized by $D$ for $V_r$, (a), while local momentum thickness $\delta_m$ is used for (b) in order to refer to the experiment by Little and Eaton (1994) for the disk rotating in a stationary ambient. The radial velocity $V_r$, (a), shows a mean velocity profile which resembles that of a plane wall jet, with a maximum velocity at $z/D \sim 0.1$. When the disk rotates, the location of the maximum velocity shifts toward the wall, as already seen in Fig. 4. At $\alpha = 4.0$, the velocity profile keeps a shape similar to that of the stationary case, though a steep peak near the wall becomes more obvious as $\alpha$ increases. For $\alpha = 16.2$, the maximum $V_r$ reaches nearly twice as much of that of the stationary case, i.e., the acceleration by which the centrifugal force dominates the wall jet. The observation on the circumferential component, $V_\theta$ in (b), discovers the fact that the present flow is still remarkably different from the boundary layer developed on the rotating disk without an impinging jet. We can see that the $V_\theta$ profile for $\alpha = 16.2$ deviates from the profiles measured at $\alpha = 4.0$ and 8.1, but the agreement with the experiment without a jet has not been achieved.

#### 4.2.2. Reynolds stresses

Fig. 6 illustrates the three normal components of the Reynolds stress: $\overline{v_r^2}$, $\overline{v_\theta^2}$, and $\overline{v_z^2}$. The influence of disk rotation on all three components is obvious; the increase in $\alpha$ results in the generation of turbulence. The most remarkable effect is seen in the $\overline{v_\theta^2}$ component. As already seen in Fig. 3(b), the increase in $\overline{v_r^2}$ at $\alpha = 16.2$ is almost five times the result without disk rotation. The increase in $\overline{v_\theta^2}$, however, is much more obvious, yielding the difference of more than an order of magnitude relative to the result without disk rotation. The reason is that in the flow without rotation, the production of $\overline{v_\theta^2}$ is zero, while the disk rotation produces a shear rate of $\partial V_\theta/\partial z$, cf. Eq. (3). As a consequence, the $\overline{v_\theta^2}$-component far exceeds the radial normal component $\overline{v_r^2}$, which would be dominant in the radial wall jet in absence of the disk rotation. Although the data for the wall-normal component, $\overline{v_z^2}$, is sparse in the near-wall region due to the blocking of laser beams by the disk, it is found that the plots for $\alpha = 16.2$ deviate from the other plots, resembling the cases in (a) and (b).

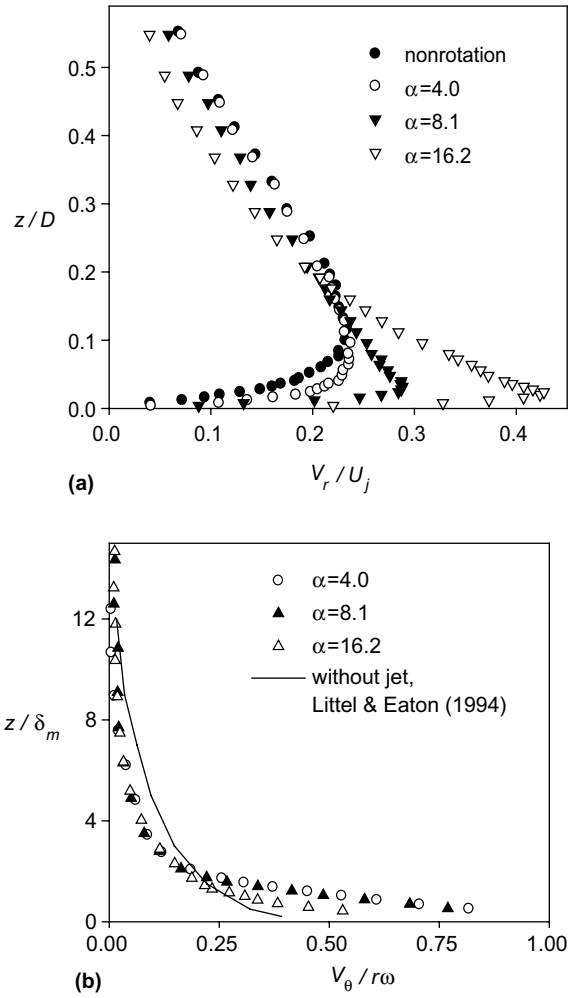


Fig. 5. Normalized mean velocity components: (a) radial component, (b) circumferential component.

The shear stress components are compared in Fig. 7. Because of the elaborate algebra required to evaluate the $\overline{v_r v_z}$-component, the ambiguity in this particular component, indicated by the error-bar in the figure, is enormous. The influence of disk rotation is weak since

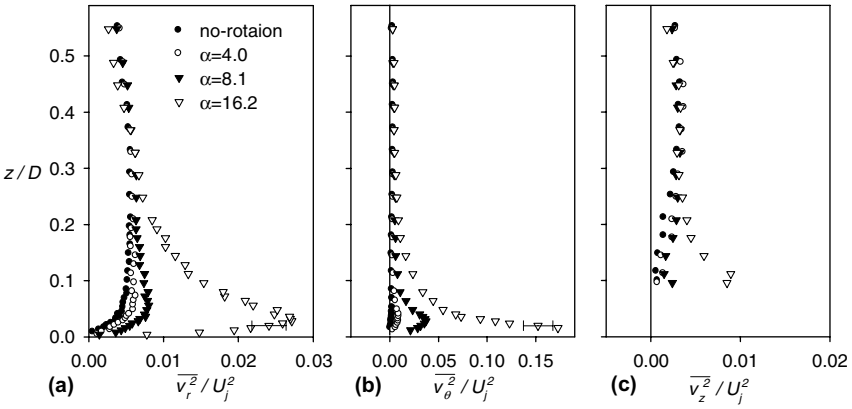


Fig. 6. Normal components of Reynolds stress.

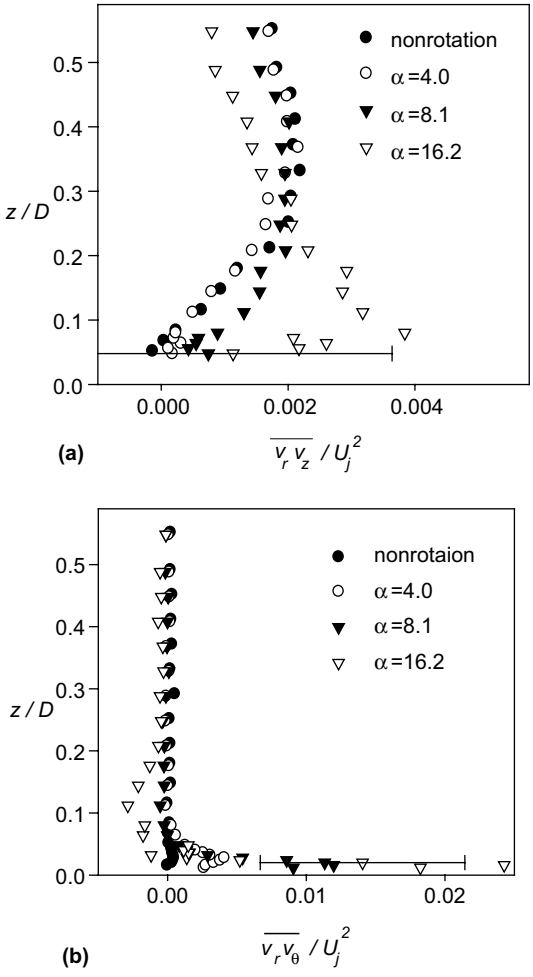


Fig. 7. Shear components of Reynolds stress: (a) $\overline{v_r v_z}$, (b) $\overline{v_r v_\theta}$.

the production of this component does not contain the direct effect, cf. Eq. (7), but still recognized in the sense that the increasing $\alpha$ provides larger turbulence. The difference between the non-rotation case and the result for $\alpha = 4.0$ is negligibly small, which is in accordance to the observation of the normal stress components. With the increasing $\alpha$, the profile gradually deviates, and at $\alpha = 16.2$, the profile is qualitatively different, with the remarkable peak observed at $z/D = 0.1$. The $\overline{v_r v_\theta}$ is absent when the disk is stationary, and therefore, should reflect more directly the influence of disk rotation as indicated by Eq. (5). Extremely large values are observed immediate to the wall when the disk rotation is applied, see Fig. 7(b).

Fig. 8 illustrates the shear stress component $\overline{v_r v_\theta}$ with respect to the local scale, $V_{r\max} r\omega$ and $\delta$. The result of the experiment without jet (Little and Eaton, 1994) is shown for reference. Because of the difference in the local tangential velocity $r\omega$, the difference due to $\alpha$ is not so large as was in Fig. 7, implying a weak similarity of the results from different $\alpha$, although the experimental uncertainty is large. In reference to the production rate $P_{r\theta}$, Eq. (5), the difference between the present case and the case without impinging jet may be explained as follows: The impinging jet drives the radial flow, hence

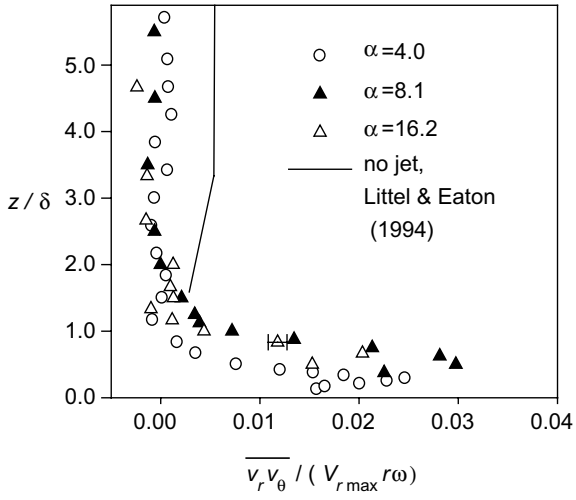


Fig. 8. Reynolds shear stress $\overline{v_r v_\theta}$ normalized by local scales.

increases the mean velocity gradient $\partial V_r/\partial z$ near the disk surface. On the other hand, the shear stress component $\overline{v_\theta v_z}$ is subject to the direct effect of the disk rotation as indicated by Eq. (6). The product of these quantities increases the production rate $P_{r\theta}$ hence results in the large value of the $\overline{v_r v_\theta}$-component as shown in Fig. 8.

The above consideration suggests that the representation of the strong anisotropy among the production rate of Reynolds stress components is the key to explain the problem. The turbulence modeling of at least second-moment level may be required for the prediction of the present flow.

## 5. Concluding remarks

We conduct the detailed measurements in the turbulent boundary layer developed on a rotating disk; this layer is where a turbulent jet impinges onto the center of the disk. The influence of rotation on the development of the radial wall jet is remarkable in both the skew in the mean flow and the centrifugal force. Based on the order of estimation of the centrifugal force in the radial momentum equation, we proposed a non-dimensional parameter $\alpha$, which correlates the radial location and the disk rotational speed so that the classification of the resulting velocity field becomes simple. We find that the modification of the turbulence structure, due to the disk rotation at high values of $\alpha$, is obvious in the increase of the normal stress component in the circumferential direction. The increase in the other stress components are found to be the consequence of the secondary effect, namely the re-distribution from the circumferential normal stress. The representation of the strong anisotropy in the production rate is important to characterize this problem.

## Acknowledgements

The authors are grateful to Prof. S. Masuda for invaluable discussions. A part of the present study was financially supported by the Ministry of Education, Science, Sports and Culture, Grant-in-Aid for Scientific Research (B), 15360100, 2003.

## References

Behnia, M., Parneix, S., Shabany, Y., Durbin, P.A., 1999. Numerical study of turbulent heat transfer in confined and unconfined impinging jets. Int. J. Heat Fluid Flow 20, 1–9.

Brodersen, S., Metzger, D.E., Fernando, H.J.S., 1996a. Flow generated by the impingement of a jet on a rotating surface: Part I—Basic flow patterns. J. Fluids Eng. 118, 61–67.

Brodersen, S., Metzger, D.E., Fernando, H.J.S., 1996b. Flow generated by the impingement of a jet on a rotating surface: Part II—Detailed flow structure and analysis. J. Fluids Eng. 118, 68–73.

Cooper, D., Jackson, D.C., Launder, B.E., Liao, G.X., 1993. Impinging jet studies for turbulence model assessment—I. Flowfield experiments. Int. J. Heat Mass Transfer 36, 2675–2684.

Craft, T.J., Graham, L.J.W., Launder, B.E., 1993. Impinging jet studies for turbulence model assessment—II. An examination of the performance of four turbulence models. Int. J. Heat Mass Transfer 36, 2685–2697.

Fuchs, W., Nobach, H., Tropea, C., 1994. Laser doppler anemometry data simulation: application to investigate the accuracy of statistical estimate. AIAA J. 32, 1883–1889.

Gardon, R., Akfirat, J.C., 1965. The role of turbulence in determining the heat-transfer characteristics of impinging jets. Int. J. Heat Mass Transfer 8, 1261–1272.

Itoh, M., Hasegawa, I., 1994. Turbulent boundary layer on a rotating disk in infinite quiescent fluid. JSME Int. J. Ser. B 37, 449–456.

Itoh, M., Okada, M., 1998. An experimental study of the radial wall jet on a rotating disk. Exp. Thermal Fluid Sci. 17, 49–56.

Little, H., Eaton, J.K., 1994. Turbulence characteristics of the boundary layer on a rotating disk. J. Fluid Mech. 266, 175–207.

Popiel, C.O., Boguslawski, L., 1974. Local heat transfer coefficients on the rotating disk in still air. Int. J. Heat Mass Transfer 18, 167–170.